Development/Plasticity/Repair

Reliable Genetic Labeling of Adult-Born Dentate Granule Cells Using *Ascl1*^{CreERT2} and *Glast*^{CreERT2} Murine Lines

Sung M. Yang,* Diego D. Alvarez,* and Alejandro F. Schinder

Laboratorio de Plasticidad Neuronal, Fundación Instituto Leloir-Instituto de Investigaciones Bioquímicas de Buenos Aires-Consejo Nacional de Investigaciones Científicas y Técnicas, Buenos Aires, C1405BWE, Argentina

Newly generated dentate granule cells (GCs) are relevant for input discrimination in the adult hippocampus. Yet, their precise contribution to information processing remains unclear. To address this question, it is essential to develop approaches to precisely label entire cohorts of adult-born GCs. In this work, we used genetically modified mice to allow conditional expression of tdTomato (Tom) in adult-born GCs and characterized their development and functional integration. *Ascl1*^{CreERT2};*CAG*^{floxStopTom} and *Glast*^{CreERT2};*CAG*^{floxStopTom} mice resulted in indelible expression of Tom in adult neural stem cells and their lineage upon tamoxifen induction. Whole-cell recordings were performed to measure intrinsic excitability, firing behavior, and afferent excitatory connectivity. Developing GCs were also staged by the expression of early and late neuronal markers. The slow development of adult-born GCs characterized here is consistent with previous reports using retroviral approaches that have revealed that a mature phenotype is typically achieved after 6–8 weeks. Our findings demonstrate that *Ascl1*^{CreERT2} and *Glast*^{CreERT2} mouse lines enable simple and reliable labeling of adult-born GC lineages within restricted time windows. Therefore, these mice greatly facilitate tagging new neurons and manipulating their activity, required for understanding adult neurogenesis in the context of network remodeling, learning, and behavior.

Key words: adult neurogenesis; electrophysiology; hippocampus; neural circuits; synaptogenesis; transgenic mice

Significance Statement

Our study shows that *Ascl1*^{CreERT2} and *Glast*^{CreERT2} mice lines can be used to label large cohorts of adult-born dentate granule cells with excellent time resolution. Neurons labeled in this manner display developmental and functional profiles that are in full agreement with previous findings using thymidine analogs and retroviral labeling, thus providing an alternative approach to tackle fundamental questions on circuit remodeling. Because of the massive neuronal targeting and the simplicity of this method, genetic labeling will contribute to expand research on adult neurogenesis.

Introduction

Adult hippocampal neurogenesis has been observed in vertebrates from birds to humans. The subgranular zone (SGZ) of the dentate gyrus (DG) contains radial glia-like neural stem cells (Type 1) with self-renewal capacity that generate fast-dividing Type 2 transit-amplifying progenitors, finally giving rise to neurons that develop and mature during several weeks (Zhao et al., 2008; Bonaguidi et al., 2012). Newly born granule cells (GCs) are incorporated into the functional neural networks of the DG, producing a significant impact on circuit plasticity (Laplagne et al., 2006; Toni et al., 2008; Gu et al., 2012; Marín-Burgin et al., 2012; Chancey et al., 2013; Temprana et al., 2015). Significant progress has been made in recent years to decipher how adult neurogenesis contributes to hippocampus-mediated brain functions (Drew et al., 2013; Piatti et al., 2013; Christian et al., 2014). However, the precise contribution of adult-born neurons to information processing is still unclear.

The field of adult neurogenesis has progressed because of technical advancements that have allowed the precise identification and manipulation of newly generated neurons among billions of preexisting neurons in the adult central nervous system. The different approaches include the more classical incorporation of nucleotide analogs, retrovirus-mediated gene transfer,

Received June 18, 2015; revised Aug. 27, 2015; accepted Oct. 8, 2015.

Author contributions: S.M.Y., D.D.A., and A.F.S. designed research; S.M.Y. and D.D.A. performed research; S.M.Y., D.D.A., and A.F.S. analyzed data; S.M.Y., D.D.A., and A.F.S. wrote the paper.

D.D.A. and S.M.Y. were supported by Consejo Nacional de Investigaciones Científicas y Técnicas fellowships. This work was supported by Argentine Agency for the Promotion of Science and Technology Grant PICT2010-1798, National Institutes of Health Grant FIRCA R03TW008607-01, and Howard Hughes Medical Institute SIRS Grant 55007652 to A.F.S. We thank Jane Johnson for *Ascl1*^{CreERT2} mice; Magdalena Götz for *Glast*^{CreERT2} mice; and Guillermo Lanuza and members of the Lanuza and the A.F.S. laboratories for insightful discussions and assistance in the maintenance and use of mouse lines.

The authors declare no competing financial interests.

*S.M.Y. and D.D.A. contributed equally to this work.

Correspondence should be addressed to Dr. Alejandro F. Schinder, Laboratorio de Plasticidad Neuronal, Fundación Instituto Leloir, Av. Patricias Argentinas 435, Buenos Aires, C1405BWE, Argentina. E-mail: aschinder@leloir.org.ar.

DOI:10.1523/JNEUROSCI.2345-15.2015

 0270-6474/15/3515379-12$15.00/0

and, more recently, genetically modified mice with specific drivers expressed in neural progenitor cells (Ming and Song, 2005; Overstreet-Wadiche et al., 2006; Zhao et al., 2006; Taupin, 2007; Dhaliwal and Lagace, 2011; Imayoshi et al., 2011; Dieni et al., 2013). Nevertheless, the need of *in vivo* studies to elucidate the role of adult-born GCs in hippocampal functions claims for the emergence of highly characterized tools that allow accurate identification and control of the activity of newly born neurons (Kropff et al., 2015).

Inducible forms of the Cre recombinase (CreERT2) expressed under Type 1 or Type 2 cell-specific promoters, such as Nestin, GFAP, or the Achaete-scute complex homolog 1 (Ascl1), have already been used for the study of adult neurogenesis (Encinas et al., 2006; Bonaguidi et al., 2012; Dieni et al., 2013). In particular, the astrocyte-specific glutamate transporter (GLAST) is expressed in GFAP$^+$ astrocytes and neural stem cells (Type 1), and it has allowed targeting fluorescent reporters to identify postnatal and adult hippocampal neurogenesis (Mori et al., 2006; Ninkovic et al., 2007; Colak et al., 2008; Temprana et al., 2015). Similarly Ascl1, a bHLH transcription factor involved in neuronal differentiation and present in Type 1 and Type 2 cells, has also been used to characterize and manipulate adult neurogenesis (Kim et al., 2007, 2011; Andersen et al., 2014; Mich et al., 2014). While several laboratories have already incorporated these tools for the study of adult neurogenesis, a detailed morpho-functional characterization as a function of neuronal age has never been done. Thus, the extent to which new GCs labeled using these methods provide information that is in agreement with previous results obtained with classical thymidine analogs and retroviral approaches remains unknown.

The aim of this work is to study development and functional integration of adult-born GCs identified using the *Glast*^{CreERT2} and *Ascl1*^{CreERT2} mouse lines, providing an assessment for the specificity of neuronal labeling and the precision of neuronal birth dating, compared with what has already been learnt from previous approaches. Both mouse lines were crossed to the *CAG*$^{floxStop\text{-}tdTomato}$ conditional reporter line to achieve indelible expression of tdTomato (Tom) in adult-born GCs after tamoxifen (TAM) administration. TAM induction resulted in efficient labeling of entire cohorts of new GCs in both mice lines, with some degree of transgene expression also in the progeny of slowly dividing Type 1 neural stem cells. As expected, Tom$^+$ astrocytes were also observed in *Glast*^{CreERT2} mice. Nevertheless, whole-cell recordings obtained in acute slices from mice at 21 to 56 d post induction (dpi) revealed that development of intrinsic properties, firing behavior and afferent excitatory connectivity is very similar to what has been previously reported. Furthermore, analysis of expression of doublecortin (DCX) and calbindin (Cb) also strengthens the distinctive maturation pattern of adult-born GCs. Overall, our results demonstrate that both *Glast*^{CreERT2} and *Ascl1*^{CreERT2} lines are powerful tools to label and manipulate temporally enclosed populations of adult-born GCs.

Materials and Methods

Mice

Ascl1^{CreERT2} (*Ascl1*$^{tm1(Cre/ERT2)Jejo}$/J) mice (Kim et al., 2007), obtained from The Jackson Laboratory, and *CAG*$^{floxStop\text{-}tdTomato}$ (Ai14) (B6;129S6-*Gt(ROSA)26Sor*$^{tm14(CAG\text{-}tdTomato)Hze}$/J) conditional reporter line (Madisen et al., 2010), obtained from Hongkui Zeng, were crossed to generate *Ascl1*^{CreERT2}; *CAG*^{FloxStopTom} mice. *Glast*^{CreERT2} mice (Mori et al., 2006), kindly provided by M. Götz, were crossed to *CAG*$^{floxStop\text{-}tdTomato}$ (Ai14) (B6; 129S6-*Gt(ROSA)26Sor*$^{tm14(CAG\text{-}tdTomato)Hze}$/J) conditional reporter line (Madisen et al., 2010), obtained from Hongkui Zeng, to generate *Glast*^{CreERT2};*CAG*^{floxStopTom} mice. Mice were maintained in C57Bl/6J background.

Young adult mice of either sex were used at 6–7 weeks of age, housed at 2–4 mice per cage. Running wheel housing started 2–4 d before TAM induction and continued until the day of slice preparation. Running-wheel housing was selected primarily to reproduce the conditions that we have previously used for studying retrovirally labeled GCs. TAM was delivered intraperitoneally at 50 μg/g/d for 2 consecutive days (*Glast*^{CreERT2};*CAG*^{floxStopTom}) or 120 μg/g/injection, four injections in 2 consecutive days (*Ascl1*^{CreERT2};*CAG*^{floxStopTom}) to achieve indelible expression of Tom in adult-born GCs. Mice were killed at the indicated times after TAM induction. Right hemispheres were used for acute slice preparation, and left hemispheres were fixed for further neuronal marker analysis. Experimental protocols were approved by the Institutional Animal Care and Use Committee of the Leloir Institute according to the Principles for Biomedical Research involving animals of the Council for International Organizations for Medical Sciences and provisions stated in the Guide for the Care and Use of Laboratory Animals.

Electrophysiological recordings

Slice preparation. Experiments were performed in 173 neurons from 19 mice for *Glast*^{CreERT2};*CAG*^{floxStopTom} line and 231 neurons from 27 mice for *Ascl1*^{CreERT2};*CAG*^{floxStopTom} line. Mice were anesthetized and decapitated at 21–56 d post TAM induction (dpi), and transverse slices were prepared as described previously (Marín-Burgin et al., 2012). Brains were removed into a chilled solution containing the following (in mM): 110 choline-Cl$^-$, 2.5 KCl, 2 NaH_2PO_4, 25 $NaHCO_3$, 0.5 $CaCl_2$, 7 $MgCl_2$, 20 dextrose, 1.3 Na^+-ascorbate, 0.6 Na^+-pyruvate, and 4 kynurenic acid. The right hippocampus was dissected, and slices of septal pole (400 μm thick) were cut in a vibratome (Leica VT1200 S) and transferred to a chamber containing ACSF (in mM) as follows: 125 NaCl, 2.5 KCl, 2 NaH_2PO_4, 25 $NaHCO_3$, 2 $CaCl_2$, 1.3 $MgCl_2$, 1.3 Na^+-ascorbate, 3.1 Na^+-pyruvate, and 10 dextrose (315 mOsm). Slices were bubbled with 95% O_2/5% CO_2 and maintained at 30°C for at least 1 h before experiments started.

Electrophysiology. Whole-cell recordings were performed at room temperature (23 ± 2°C) using microelectrodes (4–6 MΩ) filled with the following (mM): 150 K-gluconate, 4 $MgCl_2$, 0.1 EGTA, 1 NaCl, 10 HEPES, 4 ATP-Tris, 0.3 GTP-Tris, 10 phosphocreatine, pH 7.3, and 290 mOsm. All recordings were obtained using Axopatch 200B amplifier (Molecular Devices), digitized (Digidata 1322A, Molecular Devices), and acquired at 10–20 kHz onto a personal computer using the pClamp 9 software (Molecular Devices). Developing neurons expressing Tom were binned in the following age groups: 21–23 dpi ("22 dpi"), 24–26 dpi ("25 dpi"), 27–29 dpi ("28 dpi"), 30–41 dpi ("35 dpi"), and 42–56 dpi ("49 dpi"). Recorded neurons were visually identified in the granule cell layer by fluorescence (FITC fluorescence optics; DMLFS, Leica) and/or infrared DIC videomicroscopy.

In previous work, we have compared mature neurons born in 15-day-old embryos (which populate the outer granule cell layer), 7-day-old pups, and adult mice, finding no functional differences among neuronal groups (Laplagne et al., 2006). Therefore, unlabeled neurons localized in the outer third of the granule cell layer were selected here as mature controls. Whole-cell voltage-clamp recordings were performed at a holding potential (V_h) of −70 mV. Criteria to include cells in the analysis were visual confirmation of Tom in the pipette tip, attachment of the labeled soma to the pipette when suction is performed, and absolute leak current <100 pA at V_h. Series resistance was typically 10–20 MΩ, and experiments were discarded if >25 MΩ. Membrane capacitance and input resistance were obtained from current traces evoked by a hyperpolarizing step (10 mV, 100 ms). In current-clamp recordings, the resting membrane potential was kept at −70 mV by passing a holding current. The threshold current for spiking was assessed by successive depolarizing current steps (10 pA; 500 ms) to drive the membrane potential (V_m) from resting to 0 mV. Spontaneous excitatory postsynpatic currents (EPSC) were also recorded at a holding potential of −70 mV.

Data analysis. Analysis of electrophysiological recordings was performed off-line using in-house made MATLAB routines (The MathWorks). Action potential (AP) threshold was defined as the point at

which the derivative of the membrane potential dVm/dt was 5 mV/ms (data not shown). AP amplitude was measured from threshold to positive peak and after-hyperpolarization (AHP) amplitude, from threshold to negative peak during repolarization. Current threshold was calculated as the mean between the current step that elicited the first spike (often >1 spike) and the last stimulus that did not evoke spikes. Time between consecutive spikes ($\Delta T_{interspike}$) was measured from peak to peak. Unless otherwise specified, data are presented as mean ± SEM.

Immunofluorescence

Immunostaining was done on 60 μm free-floating coronal sections throughout the brain. Antibodies were applied in TBS with 3% donkey serum and 0.25% Triton X-100. Immunofluorescence was performed using the following primary antibodies: calbindin D-28k (Cb, rabbit polyclonal; 1:1000; Swant), DCX (goat polyclonal; 1:100; Santa Cruz Biotechnology), NeuN (mouse monoclonal; 1:50; a gift from F. H. Gage), RFP (rabbit polyclonal; 1:500; Rockland Immunochemicals), and Sox2 (goat polyclonal, 1:500; Santa Cruz Biotechnology). For Cb immunolabeling, preincubation with methanol (15 min) was included to enhance penetrability. The following corresponding secondary antibodies were used: donkey anti-mouse Cy5, donkey anti-rabbit Cy5, donkey anti-rabbit Cy3, and donkey anti-goat Cy5 (1:250; Jackson ImmunoResearch Laboratories).

Confocal microscopy

Only sections containing the septal region of the hippocampus (anteroposterior, −1.22 to −2.3 mm from bregma) according to the mouse brain atlas (Paxinos and Franklin, 2004) were included. Images were acquired using Zeiss LSM 510 Meta or Zeiss LSM 710 confocal microscopes (Carl Zeiss). Only Tom^+ cells located in the granule cell layer were included in the analysis. Analysis of neuronal marker expression was restricted to cells with fluorescence intensity levels that enabled clear identification of their somata. Images were acquired (40×; NA 1.3) from 60-μm-thick sections, taking *z*-series, including typically 20–30 optical slices, airy unit = 1 at 1 μm intervals. Marker expression analysis was performed using single optical planes and 3D reconstructions obtained from *z*-stacks. For images showing morphology, an anti-RFP antibody was used.

Numerical model

We propose a deterministic numerical model, in which the generation of labeled newborn GCs, $G(t)$, is determined as follows:

$$G(t) = (N+1)^{t/T_{\text{inflexion}}} - 1, \quad t \leq T_{\text{inflexion}}$$

$$G(t) = N \cdot e^{-t/\tau_{\text{neurogenesis}}} \quad t > T_{\text{inflexion}}$$

where t is the time after TAM induction (in dpi) and N is the number of cells born at $T_{\text{inflexion}}$ (the calculation was done with $N = 1000$, but the whole set of results are presented after normalization). The only two free parameters of this model are $T_{\text{inflexion}}$ and $\tau_{\text{neurogenesis}}$; they were adjusted to best fit our data related to expression of neuronal markers. $G(t)$, the number of newborn GCs generated at t-dpi, is a function that represents a continuous division of neuronal progenitors, starting at zero the day of the TAM injection and with an exponential decay after reaching a peak at $T_{inflexion}$ (see Fig. 5*A*). This generation was constrained by the survival probability S_n, which is associated with cell apoptosis as follows:

$$S(n) = S_0 + (1 - S_0) \cdot e^{-n/\tau_{\text{survival}}}$$

where n is the cell age. The parameters were fixed in $S_0 = 0.2$ and $\tau_{\text{survival}} = 4$ d, and they were obtained after fitting experimental data (Brandt et al., 2003). The combination of the generation rate and the survival probability leads to the total number of newborn GCs as follows:

$$N(t, n) = G(t - n) \cdot S(n)$$

In other words, the number of neurons $N(t,n)$ whose age is n at the time t is the number of neurons born n days before t, modulated by the survival probability of n-day old neurons (see Fig. 5*B*). In addition, we propose that each neuron expresses independently DCX or Cb with a probability represented by respective sigmoid functions (see Fig. 5*C*):

$$DCX(n) = 1 - \frac{1}{1 + e^{\frac{-(n-21)}{2.5}}}$$

$$Cb(n) = \frac{1}{1 + e^{\frac{-(n-19)}{2.5}}}$$

where n is expressed in days. The parameters were fixed according to experimental data (Espósito et al., 2005; Piatti et al., 2011). Finally, the total number of newborn cells expressing the neuronal marker DCX in a t-dpi animal was calculated as follows:

$$DCX\ expression(t) = \sum_{n=8}^{n=t} N(t, n) \cdot DCX(n)$$

The calculation is analogous for Cb. We started the count from 8-day-old cells because the identification of younger GCs in an experiment is unlikely. After performing optimization of the free parameters in the model, we found that the best set to fit our experimental data are $T_{\text{inflexion}} = 1$ d and $\tau_{\text{neurogenesis}} = 5$d; thus, we showed the results under this condition (see Fig. 5*D*).

Results

To characterize GCs generated in the adult hippocampus, *Ascl1*^{CreERT2} and *Glast*^{CreERT2} mice carrying the Tom allele were induced by TAM injection at 6–7 weeks of age. Neuronal phenotype was assessed by the expression of specific neuronal markers, and neuronal function was monitored by whole-cell patch-clamp recording performed in Tom^+ cells in acute brain slices prepared 21–56 d after TAM induction. Both approaches converged in the existence of distinctive stages of neuronal maturation with similar profile to that previously observed by retroviral labeling.

Functional characterization of adult-born GCs in *Ascl1*^{CreERT2} mice

In the *Ascl1*^{CreERT2} knockin mouse line used here, TAM administration elicits Cre-mediated recombination in Type 1 neural stem cells and Type 2 progenitors in the adult hippocampus (Kim et al., 2011). After slice preparation from *Ascl1*^{CreERT2};*CAG*^{floxStopTom} mice, intrinsic properties, spiking, and excitatory inputs were investigated by electrophysiological recordings in GCs with indelible expression of Tom, at variable intervals after TAM induction (Fig. 1*A*,*B*). Tom^+ GCs were compared with unlabeled mature GCs in the outer granule cell layer, mostly generated during perinatal development. The following passive membrane properties were monitored: input resistance (R_{input}), reflecting the cell size and the density of ion channels open at resting; membrane capacitance (C_m), proportional to the area of the soma and proximal dendrites; and resting potential (V_{rest}), determined by the relative ionic concentrations and permeabilities.

Neurons recorded at early intervals displayed high R_{input}, low C_m, and depolarized V_{rest}, properties that are typical of immature neurons in the developing and adult brain (Fig. 1*C*–*E*) (Owens et al., 1996; Espósito et al., 2005; Overstreet Wadiche et al., 2005; Ye et al., 2005). Over time, R_{input} decreased, C_m increased, and V_{rest} became more hyperpolarized, reaching levels characteristic of mature GCs. The whole set of intrinsic properties under study progressed in a gradual way along the different groups (Fig. 1*C*–*E*). Furthermore, the mean values for each group are consistent with those observed using retroviral labeling in adult-born GCs of related ages (Espósito et al., 2005; Mongiat et al., 2009; Gu et

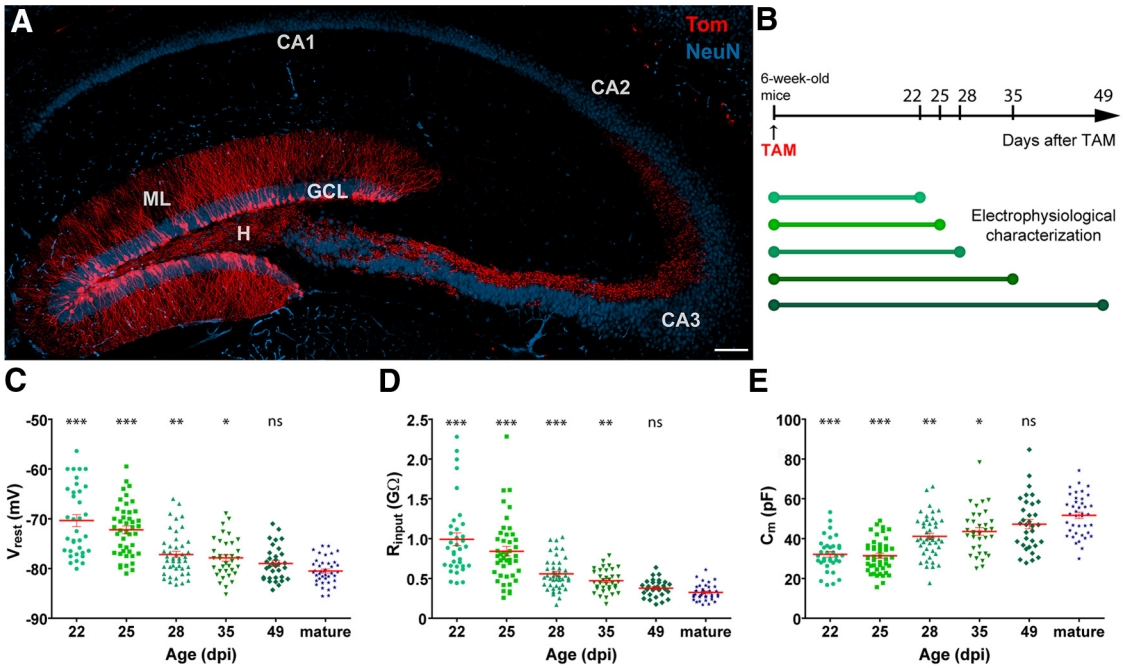

Figure 1. Intrinsic membrane properties of developing GCs generated in adult *Ascl1*^{CreERT2} mice. ***A***, Confocal image of a 60-μm-thick hippocampal section depicting adult-born GCs (red) at 49 d after TAM injection (dpi). NeuN immunofluorescence (blue) allows visualizing the GCL and CA1, CA2, and CA3 pyramidal layers. Dendrites extend through the molecular layer (ML), and mossy fibers project across the hilus (H) to CA3, via the stratum lucidum. Scale bar, 100 μm. ***B***, Tom indelible expression was induced by TAM administration, and mice were killed at different times post injection to perform electrophysiological recordings in acute slices. ***C–E***, Resting potential (***C***), input resistance (***D***), and membrane capacitance (***E***) were measured in Tom$^+$ adult-born neurons and unlabeled mature GCs. Sample sizes (presented as neurons/mice) were 35/6 (22 dpi), 44/5 (25 dpi), 44/6 (28 dpi), 35/5 (35 dpi), 33/5 (49 dpi), and 40/23 (mature). ***$p < 0.001$ compared with mature GCs. **$p < 0.01$ compared with mature GCs. *$p < 0.05$ compared with mature GCs. ns, Not significant. Red lines indicate mean ± SEM. Statistical comparisons were done using Kruskal-Wallis test followed by a *post hoc* Dunn's test.

al., 2012). No significant differences were observed for any of the parameters between the "49 dpi" group and mature GCs.

All recorded Tom$^+$ cells were identified as neurons by their capacity to generate APs. Depolarizing current injections evoked multiple spikes with different properties (number and shape) among groups (Fig. 2*A*). When analyzing spike number versus stimulus strength, the two younger groups (22 and 25 dpi) fired with high efficacy but quickly reached frequency accommodation, whereas older GCs displayed almost linear increments in the number of APs (Fig. 2*B*). Interestingly, GCs from "28 dpi" and "35 dpi" groups fired with higher efficacy than older groups for all stimuli, as a consequence of the combination of elevated R_{input} and advanced degree of maturation of voltage-gated sodium and potassium currents (Espósito et al., 2005; Mongiat et al., 2009). The gradual decrease in membrane excitability was also reflected in the current threshold to elicit the first spike, which increased gradually with the time after induction (Fig. 2*C*).

The first spike of each trial remained unchanged over GC age in regard to amplitude and half-width, whereas AHP amplitude increased gradually with the time after injection, reflecting the maturation of potassium channel populations required for repetitive firing (Fig. 2*D*). Time-dependent AP maturation was also evident by pooling all spikes in a train, revealing age-dependent increase in AP and AHP amplitudes, with concomitant decrease in AP half-width (Fig. 2*E*).

To evaluate circuit integration, voltage-clamp recordings were performed in Tom$^+$ GCs to monitor spontaneous EPSCs (sEPSCs) (Fig. 3*A*). sEPSCs were detected in all GCs, although the level of activity displayed a marked age-dependent increase (Fig. 3*B*). Interestingly, sEPSC frequency was lower at 49 dpi compared with unlabeled mature GCs, in contrast to what was observed for intrinsic properties and spiking characteristics. This result suggests a difference in functional connectivity between mature GCs born in developing versus adult hippocampus that was previously unreported.

The lower sEPSC frequency in younger GCs with no differences in amplitude or kinetic parameters suggest presynaptic rather than postsynaptic differences (Fig. 3*C*,*D*). Most likely, the time-dependent increase in postsynaptic responsiveness arises from an increment in the number of functional synaptic contacts, which has also been found at the structural level as increased number of dendritic spines (Zhao et al., 2006; Toni et al., 2008). Overall, functional properties in Tom-labeled GCs in the *Ascl1*^{CreERT2};*CAG*^{floxStopTom} indicate that time after TAM injection accurately reflects the mean age of tagged GCs.

Expression of neuronal markers in adult-born GCs in *Ascl1*^{CreERT2} mice

In addition to the electrophysiological characterization, the degree of neuronal maturity was also determined by expression of the early and late neuronal markers DCX and Cb (Piatti et al., 2011). In the same mice in which the right hippocampus was used for functional experiments, the contralateral hemisphere was fixed to assess phenotypic analysis of Tom-labeled cells using those neuronal markers. In regard to morphological progression, initially (3 dpi) Tom$^+$ cells displayed typical radial glia-like morphology (Bonaguidi et al., 2011). With age, typical neuronal features became apparent, with increased complexity in the dendritic tree (Fig. 4*A*). The number of Tom$^+$ cells increased substantially during the first few days after TAM administration, consistent with the expected amplification of Type 2 cells. Notably, fluorescence intensity of Tom$^+$ cells also increased as a func-

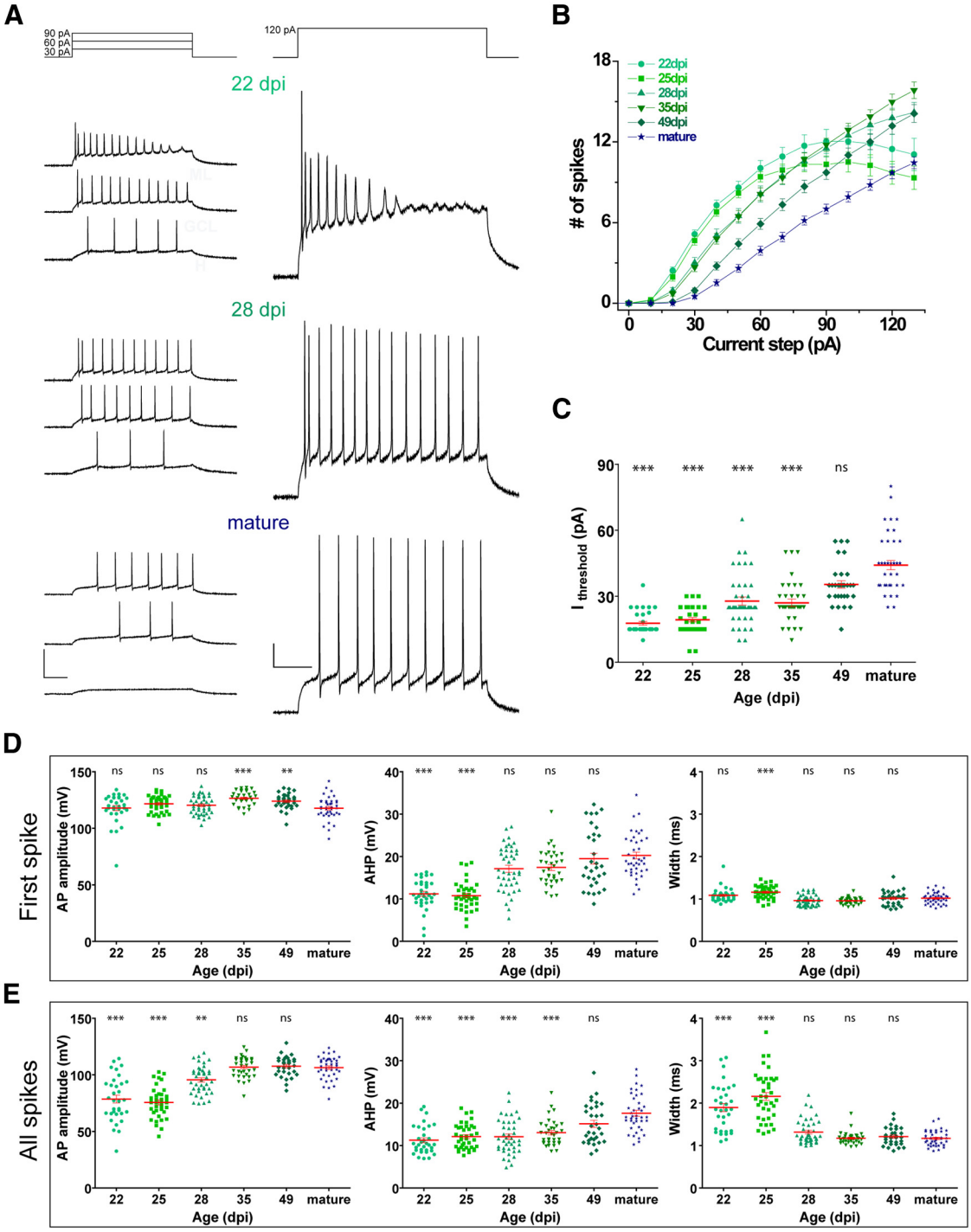

Figure 2. Spiking properties of adult-born GCs in *Ascl1*^{CreERT2} mice. ***A***, Representative whole-cell current-clamp recordings in GCs at different ages. Spiking was elicited by depolarizing current steps of increasing amplitude (500 ms, 0–130 pA, 10 pA steps). Panels represent example traces at the indicated current steps. Calibration: left, 100 mV; right, 20 mV; 100 ms. ***B***, Repetitive firing quantified as the number of spikes elicited by increasing current steps. ***C***, Current threshold to elicit the first spike for the experiments shown in ***B***. ***D***, ***E***, AP amplitude, AHP amplitude, and AP half-width were measured for the first spike (***D***) and all identified spikes (***E***). ***$p < 0.001$ compared with mature GCs. **$p < 0.01$ compared with mature GCs. *$p < 0.05$ compared with mature GCs. ns, Not significant. Sample sizes (presented as neurons/mice) were 34/6 (22 dpi), 39/5 (25 dpi), 42/6 (28 dpi), 35/5 (35 dpi), 31/5 (49 dpi), and 40/23 (mature). Red lines indicate mean ± SEM. Statistical comparisons were done using Kruskal-Wallis test followed by a *post hoc* Dunn's test.

tion of age (Fig. 4*B*). At later time points, mixed populations of labeled cells bearing high and low Tom intensities were observed, which might result from the continuous generation of GCs from slowly dividing neural stem cells. To determine the proportion of Type 1/Type 2 cells versus neurons, we monitored the expression of Sox2 (present in neural stem cells and transient amplifying progenitors) and the neuronal marker NeuN during the early time after induction (Fig. 4*C*). Interestingly, Sox2 and NeuN levels basically mirrored each other, rendering substantial decrease of the neural stem/progenitor cell population and a rapid increase in neuronal production (>50% neurogenesis by 8 d).

Neuronal maturation became evident at later time points. The proportion of Tom$^+$ cells expressing DCX decreased with GC age and, at the same time, Cb expression increased as a

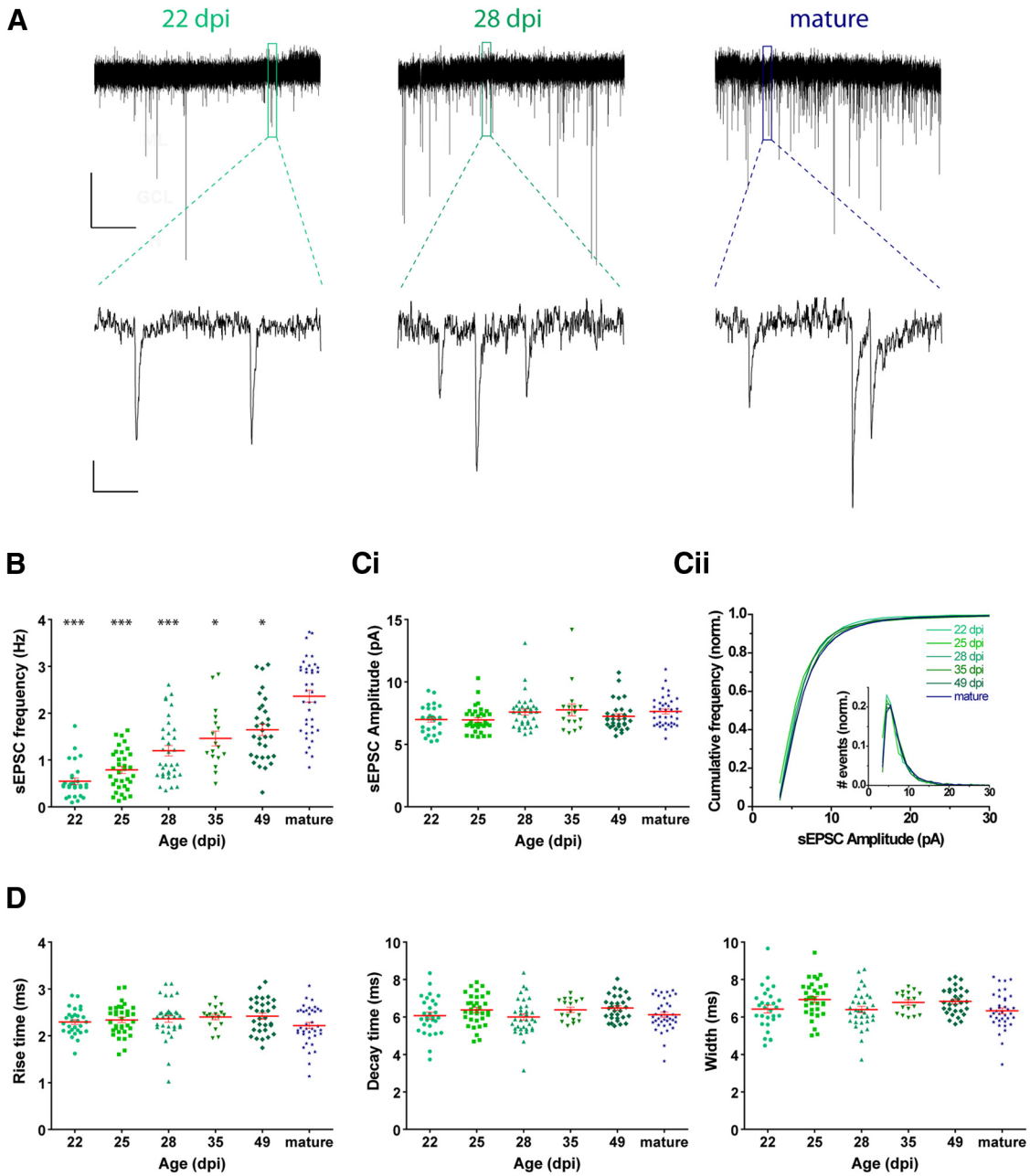

Figure 3. Excitatory input connectivity of adult-born GCs in *Ascl1*^{CreERT2} mice. ***A***, Representative traces of sEPSC recorded at −70 mV in GCs at different ages. Top, Time-compressed traces allow the visualization of sEPSC frequency. Bottom, Expanded presentations show individual events. Calibration: top, 10 pA, 10 s; bottom, 2 pA, 100 ms. ***B***, Frequency of sEPSC events, measured during 120 s. ***$p < 0.001$ compared with mature GCs (Kruskal–Wallis test followed by a *post hoc* Dunn's test). **$p < 0.01$ compared with mature GCs (Kruskal–Wallis test followed by a *post hoc* Dunn's test). *$p < 0.05$ compared with mature GCs (Kruskal–Wallis test followed by a *post hoc* Dunn's test). ***C***, sEPSC amplitude presented as mean value for each cell (***Ci***), and cumulative frequency for each cell age (***Cii***). Inset in ***Cii*** depicts amplitude histogram. Errors bars in ***Cii*** were omitted for clarity. Cumulative frequencies presented no differences with mature GCs by Kolmogorov–Smirnov test (minimum $p > 0.24$). ***D***, Kinetic analysis of sEPSCs: rise time (20%–90%), decay time (90%–30%), and half-width. No significant differences were found for any of the parameters by Kruskal–Wallis test (amplitude, $p = 0.06$; rise time, $p = 0.32$; decay time, $p = 0.10$; width, $p = 0.04$). Sample sizes (presented as neurons/mice) were 29/6 (22 dpi), 34/5 (25 dpi), 34/6 (28 dpi), 17/3 (35 dpi), 31/5 (49 dpi), and 38/22 (mature). Red lines indicate mean ± SEM.

result of the time-dependent maturation of neuronal phenotype, in agreement with the electrophysiological data (Fig. 4*D*). For instance, Cb expression reached saturation at 35 dpi, whereas DCX was completely absent by 49 dpi. These data are also highly consistent with previous findings on neuronal maturation primarily obtained with thymidine analogs and retroviral labeling (Kempermann et al., 2003; Espósito et al., 2005; Overstreet Wadiche et al., 2005; Piatti et al., 2006; Zhao et al., 2008; Piatti et al., 2011).

Because TAM induction labels mixed populations of fast (Type 2) and slowly dividing cells (Type 1), we developed a mathematical model to describe the dynamics of Tom$^+$ GCs after TAM injection in *Ascl1*^{CreERT2};*CAG*^{floxStopTom} mice. We proposed that the generation of neurons peak at 1 d after TAM induction and decay swiftly (exponential decay time of 5 d). The combination of the generation rate and a survival probability function resulted in a given time course for the number of newborn cells (Fig. 5*A*,*B*). In addition, the expression of neuronal markers was

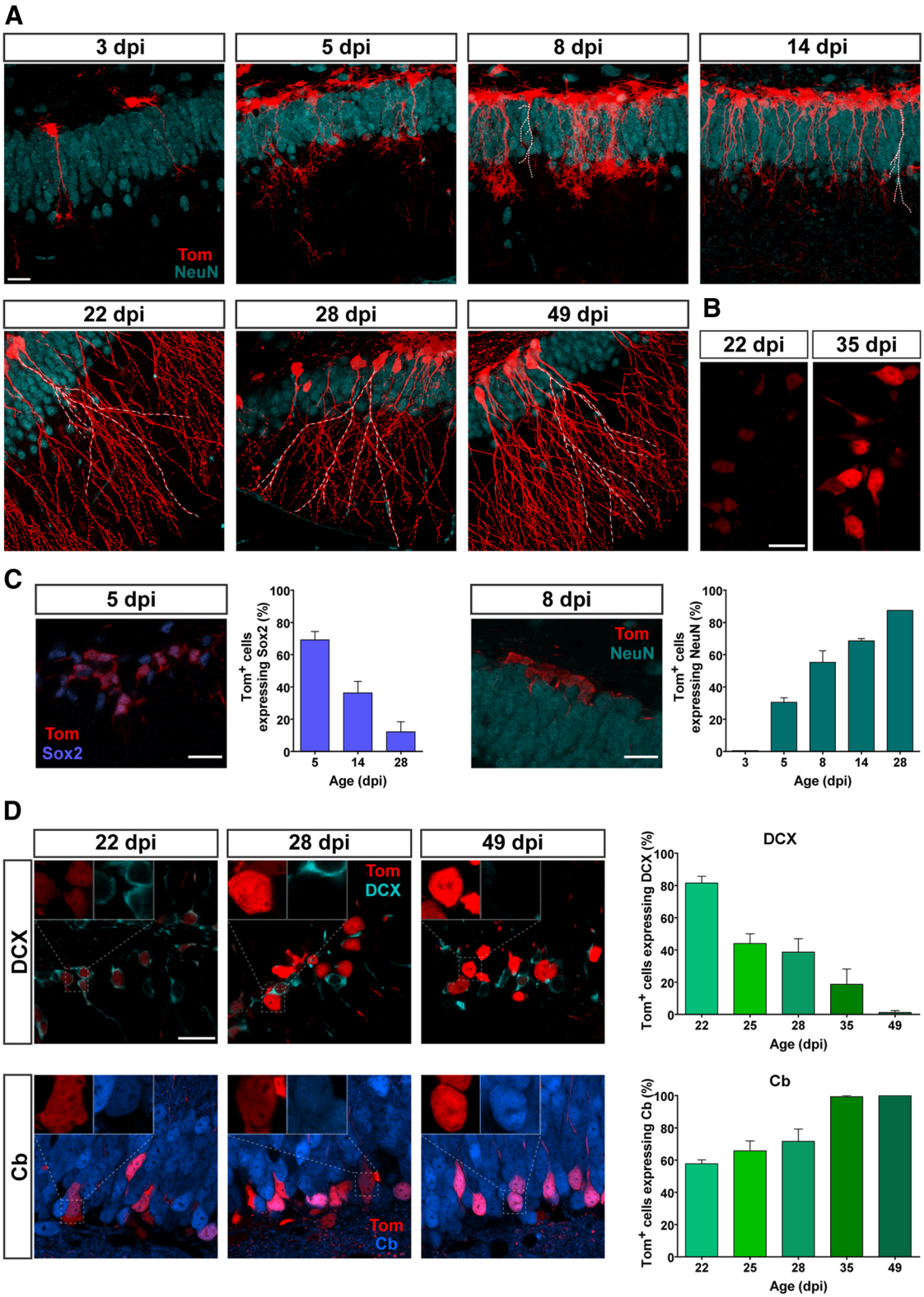

Figure 4. Morphology and neuronal markers for developing GCs generated in adult *Ascl1*^{CreERT2} mice. ***A***, Confocal images of Tom $^{+}$ cells in the dentate gyrus of *Ascl1*^{CreERT2};*CAG*^{floxStopTom} mice at different times after TAM induction. NeuN immunolabeling was performed to allow the identification of the GCL. Note the rise in the number of labeled cells from 3 to 14 dpi, characteristic of cell proliferation. White dashed lines were added to facilitate visualization of dendrites among densely packed tagged neurons. Imaging conditions were selected to render similar fluorescence intensity in all age groups. ***B***, Examples of 22 and 35 dpi GCs obtained with identical imaging settings reveal a time-dependent increase in fluorescence intensity. Note the mixed population of high and low Tom intensities at 35 dpi. ***C***, Representative images of single optical sections, and quantification of Sox2 (left) and NeuN (right) levels. Sample sizes: $>$50 Tom $^{+}$ cells, with 2 mice for each time point (1 mouse for 28 dpi). ***D***, Left, Representative images display single optical sections of DCX (top) and Cb (bottom) expression in Tom $^{+}$ GCs at different times after induction. Inset, Higher magnification of Tom $^{+}$ cells, to assess colocalization with DCX or Cb. Right, Quantification of DCX (top) and Cb (bottom) levels. Sample sizes: $>$ 90 Tom $^{+}$ GCs, with 2 or 3 mice for each time point. Error bars indicate mean $\pm$ SEM. All scale bars represent 20 μm.

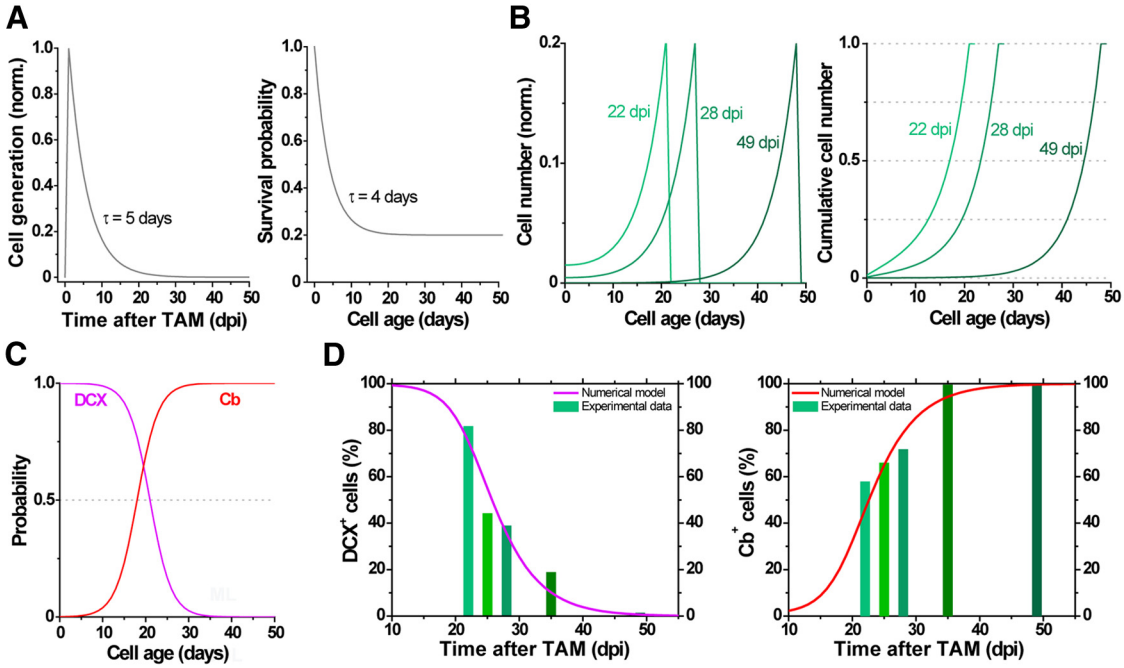

Figure 5. Computational simulation of adult neurogenesis in *Ascl1*^{CreERT2} mice. Neurogenesis results from the combination of a generation rate of newborn GCs (***A***, left; $G(t)$) and their survival probability (***A***, right; $S(n)$). Generation was represented by an exponential function starting at 1 dpi ($T_{inflexion}$) with a decay time of 5 d ($\tau_{neurogenesis}$). $T_{inflexion}$ and $\tau_{neurogenesis}$ were the only free parameters in the model. Survival probability was calculated based on experimental data (Brandt et al., 2003). The generation rate depends on the time after TAM induction, whereas the survival probability is a function of cell age. The number of newborn cells $N(t, n)$ whose age is n at the time t was calculated as $N(t, n) = G(t - n) \times S(n)$. The population of GCs at different times after TAM induction has a substantial contribution of neurons whose age is close to the time after induction (***B***). To compute the expression of neuronal markers, we assumed that each labeled cell independently expresses DCX or Cb with a probability represented by respective sigmoid functions (***C***), according to previous experimental data (Espósito et al., 2005; Piatti et al., 2011). The model predicts expression levels of DCX (***D***, left, violet line) and Cb (***D***, right, red line) tightly close to experimental data (green bars, extracted from Fig. 4). For details on the model, see also Materials and Methods.

computed by means of respective probability function for each cell to present independently DCX or Cb (Fig. 5*C*). In this way, the model rendered time-enclosed groups of new GCs, predicting expression levels of DCX and Cb with good correspondence to the experimental observations (Fig. 5*D*). The model indicates that ~50% of Tom$^+$ cells correspond to an age within 5 d of TAM induction, whereas the remaining cells are younger (Fig. 5*B*, right).

We conclude that *Ascl1*^{CreERT2} mice allow reliable birth dating of newly generated GCs. Our results suggest that Tom$^+$ GCs derive from lineages of Type 1 neural stem cells and Type 2 transit amplifying progenitors. Thus, a largely enriched cohort of GCs generated at the time of TAM injection (the *wavefront* of tagged cells, most likely derived from Type 2 cells) is followed by younger cohorts of GCs born at later times (most likely derived from slowly dividing Type 1 cells).

Phenotypic characterization of adult-born GCs in *Glast*^{CreERT2} mice

The glutamate transporter GLAST is localized on the cell membrane of mature astrocytes, and it is also expressed in neural stem cells in the adult brain. For the latter reason, GLAST has been used as a marker for the study of adult neurogenesis (Bonaguidi et al., 2012; DeCarolis et al., 2013). TAM injection in *Glast*^{CreERT2}; *CAG*^{floxStopTom} mice induced Tom expression in astrocytes and adult-born GCs (Fig. 6*A*). Labeled neurons, located in the inner GCL, displayed typical dendritic arborization of GCs. Indeed, whole-cell recordings rendered mean values for intrinsic properties (R_{input}, C_m, and V_{rest}) that were very similar to those obtained for *Ascl1*^{CreERT2} mice (Fig. 6*C–E*; Table 1) and, thus, consistent with reported data in the literature for adult-born GCs of related age. Interestingly, the variance of R_{input} values (a reliable parameter that best reflects different stages of neuronal maturation) was barely larger than the dispersion observed for *Ascl1*^{CreERT2} mice (Table 1).

Current-clamp recordings in Tom$^+$ GCs were used to characterize spiking properties of new GCs in *Glast*^{CreERT2} mice (Fig. 7*A*). We analyzed the number of APs elicited by increasing current injection and stimulus threshold, as well as spike amplitude, half-width, and AHP amplitude in the first spike and all spikes together (Fig. 7*B–E*). Consistent with the passive properties, spiking characteristics also resembled *Ascl1*^{CreERT2} data. For instance, all groups displayed an increasing number of APs in response to progressive stimulus intensity, GCs of "28 dpi" group fired with higher efficacy than other groups, and the current threshold increased in a gradual way with the time after induction. In addition, both AP and AHP amplitudes increased and AP width decreased in a gradual manner with GC age. As mentioned before, this progression in spike shape suggested AP maturation. Thus, both passive and active membrane properties seemed to develop gradually, and the exhibited results are consistent with the reported data in the literature for adult-born GCs of related age.

Functional study was complemented by phenotypic marker analysis (Fig. 8). The proportion of Tom$^+$ cells expressing DCX decreased with time after induction and, at the same time, the expression of Cb increased. In general, values are comparable with reported data, although both DCX and Cb expression revealed a slightly delayed maturation compared with that observed by retroviral labeling technique and also in *Ascl1*^{CreERT2} mice. This finding is

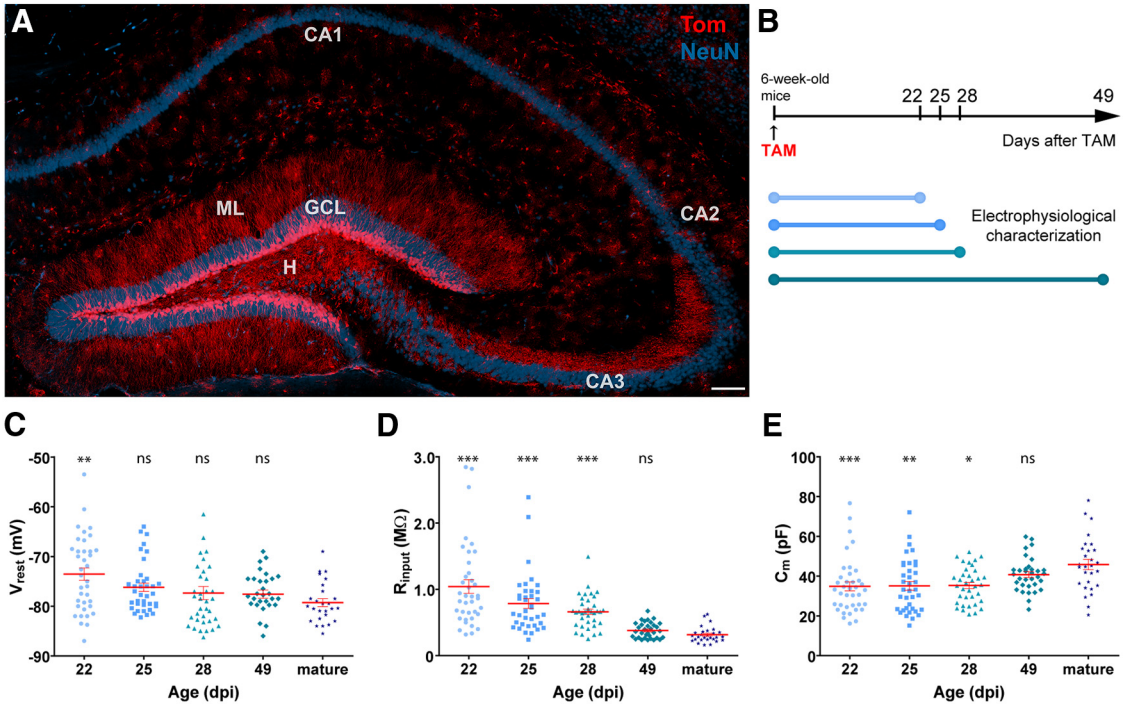

Figure 6. Intrinsic properties of adult-born GCs in *Glast*^{CreERT2} mice. ***A***, Confocal image of a 60-μm-thick hippocampal section depicting adult-born GCs (red) at 49 dpi. NeuN immunofluorescence (blue) allows visualizing the GCL, CA1, CA2, and CA3 pyramidal layers. Dendrites extend through the molecular layer (ML), and mossy fibers project across the hilus (H) to CA3, via the stratum lucidum. There are scattered Tom$^+$ astrocytes throughout the section. Scale bar, 100 μm. ***B***, Tom indelible expression was induced by TAM administration, and animals were killed at different ages to perform electrophysiological recordings in acute slices. ***C–E***, Resting potential (***C***), input resistance (***D***), and capacitance (***E***) were measured in fluorescent adult-born neurons and unlabeled mature GCs. Sample sizes (presented as neurons/mice) were 38/5 (22 dpi), 37/6 (25 dpi), 37/4 (28 dpi), 33/4 (49 dpi), and 28/19 (mature). ***$p < 0.001$ compared with mature GCs (Kruskal–Wallis test followed by a *post hoc* Dunn's test). **$p < 0.01$ compared with mature GCs (Kruskal–Wallis test followed by a *post hoc* Dunn's test). *$p < 0.05$ compared with mature GCs (Kruskal–Wallis test followed by a *post hoc* Dunn's test). ns, Not significant. Red lines indicate mean ± SEM.

Table 1. Membrane resistance in adult-born GCs labeled using different approaches[a]

	Input resistance					
					Retroviral labeling	
	Ascl1^{CreERT2} mice		Glast^{CreERT2} mice		(Mongiat et al., 2009)	(Gu et al., 2012)
Age (dpi)	Mean ± SD (MΩ)	Dispersion (%)	Mean ± SD (MΩ)	Dispersion (%)	Mean (MΩ)	Mean (MΩ)
22	990 ± 470	48	1040 ± 640	62	950	890
25	840 ± 400	47	790 ± 450	57	—	—
28	560 ± 200	36	660 ± 250	38	450	530
49	380 ± 100	26	380 ± 120	32	240	270
Mature	324 ± 95	29	310 ± 110	35	220	—

[a]Input resistance (mean ± SD) measured in *Ascl1*^{CreERT2} mice and *Glast*^{CreERT2} mice for different groups. Reported data use retroviral labeling. Dispersion was calculated as SD/mean value (%).

consistent with the labeling of a higher proportion of Type 1 cells compared with *Ascl1*^{CreERT2}-mediated labeling, which is more biased toward Type 2 cells (Kim et al., 2011; Bonaguidi et al., 2012). It is important to note that a small cohort of GCs expressing Tom were detected in sections obtained from *Glast*^{CreERT2};*CAG*^{floxStopTom} mice that did not receive TAM (nor had any contact with induced mice), indicating that CreER-dependent recombination is slightly leaky in this line. Nevertheless, the proportion of labeled cells was minor (<6%; 8.6 ± 6.8 cells/slice in noninduced mice vs 144 ± 22 cells/slice in induced mice), and thus did not alter substantially the obtained results. In contrast, Tom$^+$ cells were never observed in brain sections from *Ascl1*^{CreERT2};*CAG*^{floxStopTom} mice that did not receive TAM induction.

Overall, these data show that the population of GCs expressing Tom is largely enriched in newly generated GCs born around the time of TAM injection, highlighting both mouse lines as useful tools for studying adult neurogenesis.

Discussion

We performed functional and phenotypic characterization of adult-born GCs in *Ascl1*^{CreERT2};*CAG*^{floxStopTom} and *Glast*^{CreERT2};*CAG*^{floxStopTom} mice. The obtained results indicate that both lines allow reliable birth dating of newly generated GCs. The population of GCs expressing Tom is largely enriched in adult-born GCs generated around the time of TAM injection, with more accurate age-tagging in *Ascl1*^{CreERT2} than in *Glast*^{CreERT2} mice, with the latter displaying a slightly delayed maturation curve for new GCs. Therefore, these genetically modified mice are highly useful tools to label newly generated GCs in experimental conditions that require selective age-tagging.

Adult neurogenesis faces now an inflection point in which *in vivo* experiments are beginning to validate evidence obtained in the field over the last 20 years on the role of adult-born GCs in information processing (Drew et al., 2013; Kropff et al., 2015).

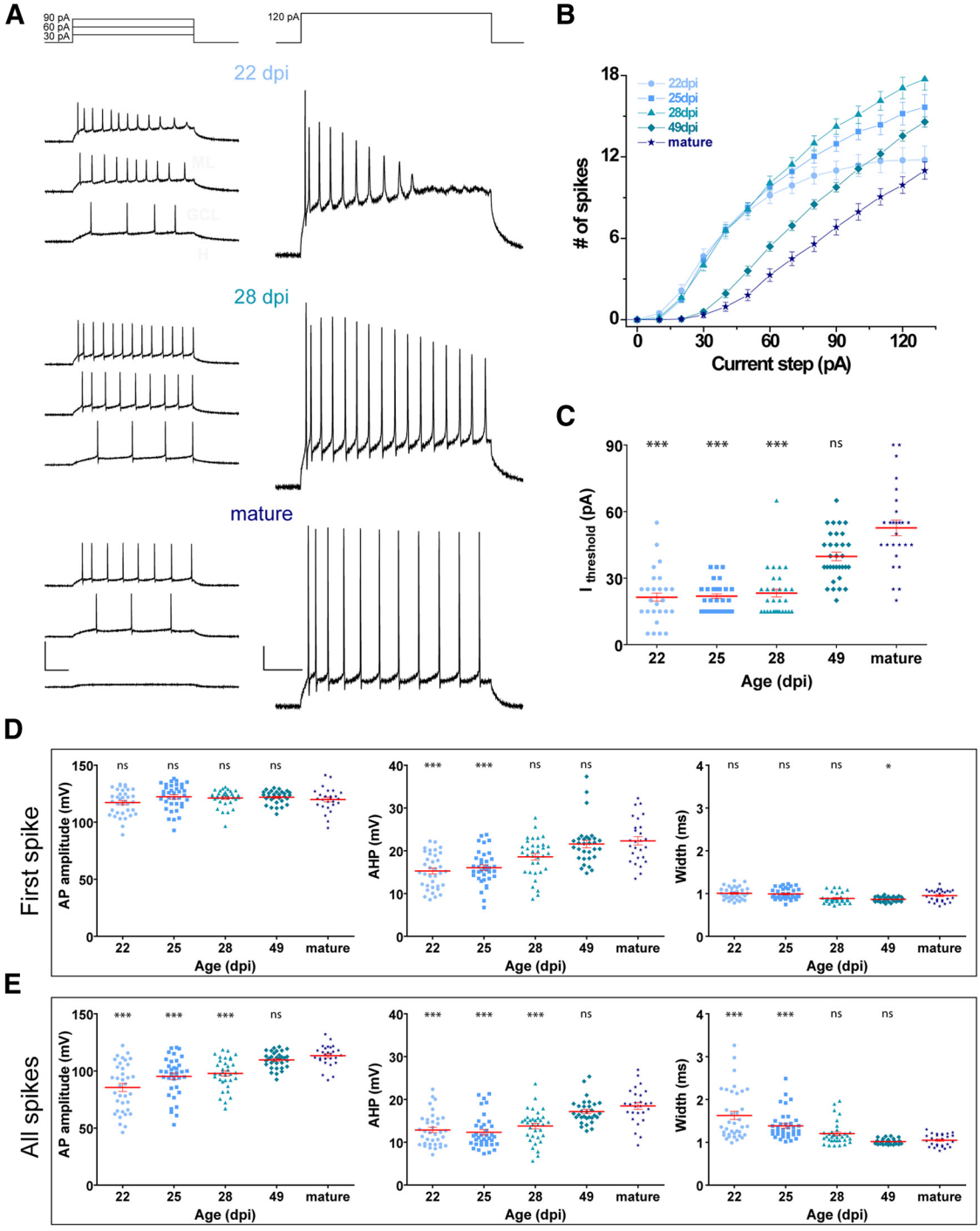

Figure 7. Spiking properties of adult-born GCs in *Glast*^{CreERT2} mice. ***A***, Representative whole-cell current-clamp recordings in GCs at different ages, as indicated. Spiking was elicited by depolarizing current steps of increasing amplitude (500 ms, 0–130 pA, 10 pA steps). Panels represent example traces at the indicated current steps. Calibration: left, 100 mV; right, 20 mV; 100 ms. ***B***, Repetitive firing quantified as the number of spikes elicited by increasing current steps. ***C***, Current threshold to elicit the first spike for the experiments shown in ***B***. ***D***, ***E***, AP amplitude, AHP amplitude, and AP half-width were measured for the first spike (***D***) and all identified spikes (***E***). ***$p < 0.001$ compared with mature GCs (Kruskal–Wallis test followed by a *post hoc* Dunn's test). **$p < 0.01$ compared with mature GCs (Kruskal–Wallis test followed by a *post hoc* Dunn's test). *$p < 0.05$ compared with mature GCs (Kruskal–Wallis test followed by a *post hoc* Dunn's test). ns, Not significant. Sample sizes (presented as neurons/mice) were 36/5 (22 dpi), 37/6 (25 dpi), 35/4 (28 dpi), 32/4 (49 dpi), and 27/16 (mature). Red lines indicate mean ± SEM.

Thymidine analogs, such as BrdU, CldU, and EdU, have long been used to label adult-born GCs (Ming and Song, 2005). Although this technique has the advantage of labeling large numbers of neurons, it does not allow monitoring cells in slice preparations or *in vivo*. Retroviral labeling has been widely used for the study of adult-born GC properties in electrophysiological slices, and it is the preferred tool for labeling enclosed cohorts of newborn GCs (Ming and Song, 2005). However, the retroviral approach has the disadvantage of labeling few neurons per animal, and those neurons are restricted to areas neighboring the injection sites. Knock-in lines in which reporter fluorophores are under the control of key promoters (e.g., Nestin^{GFP}; DCX^{GFP}) have successfully been used, but labeling is transient and, usually, fluorescent signals are weak (Hadjan-

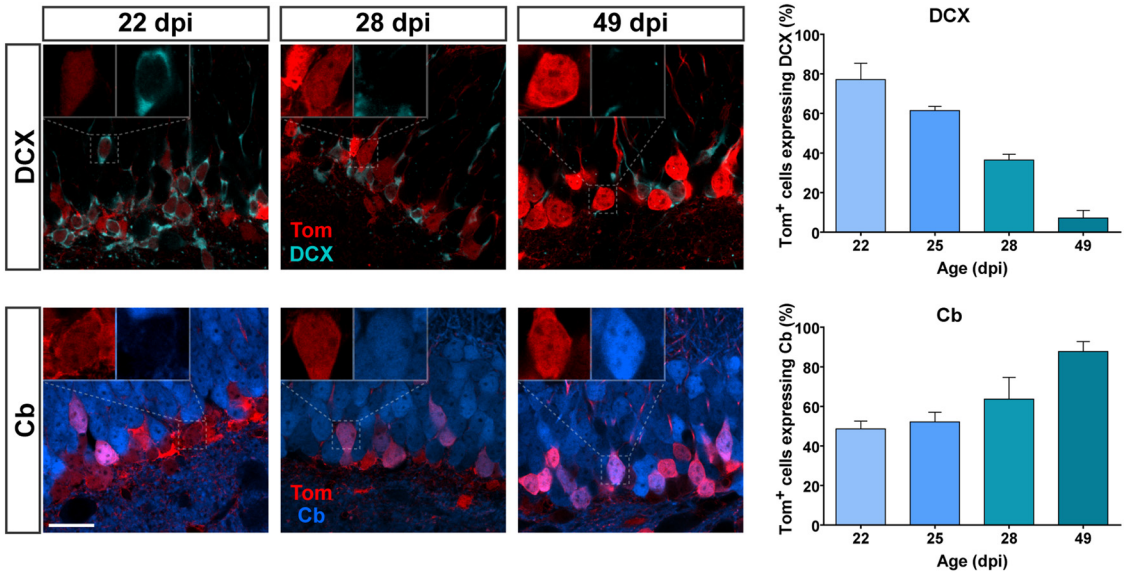

Figure 8. Neuronal markers in developing GCs generated in adult *Glast*^{CreERT2} mice. Left, Representative images display single optical sections of DCX (top) and Cb (bottom) expression in Tom$^+$ GCs at different times after induction. Inset, Higher magnification of Tom$^+$ cells allows visualizing colocalization with early or late neuronal markers. Scale bar, 20 μm. Right, Quantification of DCX (left) and Cb (right) levels. Sample sizes: >120 Tom$^+$ GCs, with 3 or 4 mice for each time point. Error bars indicate mean ± SEM.

tonakis et al., 2003; Ming and Song, 2005). Inducible forms of the Cre recombinase (CreERT2) allow controlling the onset of labeling through TAM administration with high and standardized levels of reporter expression (Madisen et al., 2010). Here we characterized adult-born GCs in two genetically modified mice lines, *Ascl1*^{CreERT2} and *Glast*^{CreERT2}, already being used to study adult neurogenesis.

Ascl1 is expressed in dividing progenitor cells and promotes their proliferation, specification, and differentiation into neurons in the adult hippocampus (Bertrand et al., 2002; Castro et al., 2011; Bonaguidi et al., 2012; Andersen et al., 2014). In *Ascl1*^{CreERT2} mice, administration of TAM induces Cre-mediated recombination in transient-amplifying and neural stem cells. Here we showed that TAM induction in *Ascl1*^{CreERT2} mice labeled a cohort of GCs within the DG that displayed the typical temporal progression of electrophysiological and phenotypic properties of adult-born GCs. The presence of radial glia-like Tom$^+$ cells during a few days after TAM administration is consistent with the expression of Ascl1 in Type 1 neural stem cells (Kim et al., 2011; Andersen et al., 2014). However, this population of cells was largely decreased 10 d after TAM injection, suggesting that labeled radial glia-like cells labeled have already been committed to enter fast divisions followed by neuronal differentiation (Kim et al., 2011; Andersen et al., 2014). We presented a simple mathematical model, whose main parameters were fitted by previous experimental data (Brandt et al., 2003; Espósito et al., 2005; Piatti et al., 2011), describing neuronal generation in *Ascl1*^{CreERT2} murine line. This model predicted very well the phenotypic data presented here, and it will be a valuable tool to design and interpret future experiments with this and other mouse lines after minor modifications. In addition, adjusting TAM induction from a single low dose to multiple injections at large doses in *Ascl1*^{CreERT2} mice may render a substantially expanded dynamic range for the number of Tom$^+$ cells, from single isolated cells (Bonaguidi et al., 2011) to thousands of neurons (data not shown). This tool will also allow detecting substantial numbers of new neurons even in mice with low rates of neuronal production, such as in aging conditions.

The glutamate aspartate transporter GLAST is highly expressed in astrocytes and radial glia-like stem cells, even in the quiescent state. TAM administration in *Glast*^{CreERT2} mice labeled astrocytes in the whole brain and adult-born neurons in the DG (Mori et al., 2006). TAM-induced Tom$^+$ GCs within the DG were easily identified by morphology and, thus, distinguished from astrocytes. Electrophysiological analysis of Tom$^+$ GCs in *Glast*^{CreERT2} mice indicated that functional characteristics were comparable with those in the *Ascl1*^{CreERT2} line and retroviral labeling (Table 1), resembling the typical maturation progress of adult-born neurons. The slightly larger dispersion observed in input resistance values for *Glast*^{CreERT2} line compared with *Ascl1*^{CreERT2} line reflects the lineage tracing from slowly dividing neural stem cells rather than Type 2 progenitors, similarly to what has been reported for the *Nestin*^{CreERT2} line (Dieni et al., 2013). Consistent with this notion, DCX and Cb analysis revealed a slight shift toward more immature states.

It is important to underline that, as a consequence of GLAST expression, *Glast*^{CreERT2} mice allow labeling of large populations of new GCs with low TAM doses. In contrast, because Ascl1 is expressed within a more restricted time window in neuronal differentiation, *Ascl1*^{CreERT2} mice require more intensive induction schemes but eventually allow single-cell fate mapping and sharper resolution in regard to neuronal age.

Well-characterized tools allow the design of reliable experiments and accurate interpretation of the data. Combined with appropriate optogenetic and chemogenetic approaches, *Ascl1*^{CreERT2} and *Glast*^{CreERT2} mice will continue to contribute in the clarification of the role of adult neurogenesis in hippocampal function, particularly, under *in vivo* conditions.

References

Andersen J, Urbán N, Achimastou A, Ito A, Simic M, Ullom K, Martynoga B, Lebel M, Göritz C, Frisén J, Nakafuku M, Guillemot F (2014) A transcriptional mechanism integrating inputs from extracellular signals to activate hippocampal stem cells. Neuron 83:1085–1097. CrossRef Medline

Bertrand N, Castro DS, Guillemot F (2002) Proneural genes and the speci-

fication of neural cell types. Nat Rev Neurosci 3:517–530. CrossRef Medline

Bonaguidi MA, Wheeler MA, Shapiro JS, Stadel RP, Sun GJ, Ming GL, Song H (2011) In vivo clonal analysis reveals self-renewing and multipotent adult neural stem cell characteristics. Cell 145:1142–1155. CrossRef Medline

Bonaguidi MA, Song J, Ming GL, Song H (2012) A unifying hypothesis on mammalian neural stem cell properties in the adult hippocampus. Curr Opin Neurobiol 22:754–761. CrossRef Medline

Brandt MD, Jessberger S, Steiner B, Kronenberg G, Reuter K, Bick-Sander A, von der Behrens W, Kempermann G (2003) Transient calretinin expression defines early postmitotic step of neuronal differentiation in adult hippocampal neurogenesis of mice. Mol Cell Neurosci 24:603–613. CrossRef Medline

Castro DS, Martynoga B, Parras C, Ramesh V, Pacary E, Johnston C, Drechsel D, Lebel-Potter M, Garcia LG, Hunt C, Dolle D, Bithell A, Ettwiller L, Buckley N, Guillemot F (2011) A novel function of the proneural factor Ascl1 in progenitor proliferation identified by genome-wide characterization of its targets. Genes Dev 25:930–945. CrossRef Medline

Chancey JH, Adlaf EW, Sapp MC, Pugh PC, Wadiche JI, Overstreet-Wadiche LS (2013) GABA depolarization is required for experience-dependent synapse unsilencing in adult-born neurons. J Neurosci 33:6614–6622. CrossRef Medline

Christian KM, Song H, Ming GL (2014) Functions and dysfunctions of adult hippocampal neurogenesis. Annu Rev Neurosci 37:243–262. CrossRef Medline

Colak D, Mori T, Brill MS, Pfeifer A, Falk S, Deng C, Monteiro R, Mummery C, Sommer L, Götz M (2008) Adult neurogenesis requires Smad4-mediated bone morphogenic protein signaling in stem cells. J Neurosci 28:434–446. CrossRef Medline

DeCarolis NA, Mechanic M, Petrik D, Carlton A, Ables JL, Malhotra S, Bachoo R, Götz M, Lagace DC, Eisch AJ (2013) In vivo contribution of nestin- and GLAST-lineage cells to adult hippocampal neurogenesis. Hippocampus 23:708–719. CrossRef Medline

Dhaliwal J, Lagace DC (2011) Visualization and genetic manipulation of adult neurogenesis using transgenic mice. Eur J Neurosci 33:1025–1036. CrossRef Medline

Dieni CV, Nietz AK, Panichi R, Wadiche JI, Overstreet-Wadiche L (2013) Distinct determinants of sparse activation during granule cell maturation. J Neurosci 33:19131–19142. CrossRef Medline

Drew LJ, Fusi S, Hen R (2013) Adult neurogenesis in the mammalian hippocampus: why the dentate gyrus? Learn Mem 20:710–729. CrossRef Medline

Encinas JM, Vaahtokari A, Enikolopov G (2006) Fluoxetine targets early progenitor cells in the adult brain. Proc Natl Acad Sci U S A 103:8233–8238. CrossRef Medline

Espósito MS, Piatti VC, Laplagne DA, Morgenstern NA, Ferrari CC, Pitossi FJ, Schinder AF (2005) Neuronal differentiation in the adult hippocampus recapitulates embryonic development. J Neurosci 25:10074–10086. CrossRef Medline

Gu Y, Arruda-Carvalho M, Wang J, Janoschka SR, Josselyn SA, Frankland PW, Ge S (2012) Optical controlling reveals time-dependent roles for adult-born dentate granule cells. Nat Neurosci 15:1700–1706. CrossRef Medline

Hadjantonakis AK, Dickinson ME, Fraser SE, Papaioannou VE (2003) Technicolour transgenics: imaging tools for functional genomics in the mouse. Nat Rev Genet 4:613–625. CrossRef Medline

Imayoshi I, Sakamoto M, Kageyama R (2011) Genetic methods to identify and manipulate newly born neurons in the adult brain. Front Neurosci 5:64. CrossRef Medline

Kempermann G, Gast D, Kronenberg G, Yamaguchi M, Gage FH (2003) Early determination and long-term persistence of adult-generated new neurons in the hippocampus of mice. Development 130:391–399. CrossRef Medline

Kim EJ, Leung CT, Reed RR, Johnson JE (2007) In vivo analysis of Ascl1 defined progenitors reveals distinct developmental dynamics during adult neurogenesis and gliogenesis. J Neurosci 27:12764–12774. CrossRef Medline

Kim EJ, Ables JL, Dickel LK, Eisch AJ, Johnson JE (2011) Ascl1 (Mash1) defines cells with long-term neurogenic potential in subgranular and subventricular zones in adult mouse brain. PLoS One 6:e18472. CrossRef Medline

Kropff E, Yang SM, Schinder AF (2015) Dynamic role of adult-born dentate granule cells in memory processing. Curr Opin Neurobiol 35:21–26. CrossRef Medline

Laplagne DA, Espósito MS, Piatti VC, Morgenstern NA, Zhao C, van Praag H, Gage FH, Schinder AF (2006) Functional convergence of neurons generated in the developing and adult hippocampus. PLoS Biol 4:e409. CrossRef Medline

Madisen L, Zwingman TA, Sunkin SM, Oh SW, Zariwala HA, Gu H, Ng LL, Palmiter RD, Hawrylycz MJ, Jones AR, Lein ES, Zeng H (2010) A robust and high-throughput Cre reporting and characterization system for the whole mouse brain. Nat Neurosci 13:133–140. CrossRef Medline

Marín-Burgin A, Mongiat LA, Pardi MB, Schinder AF (2012) Unique processing during a period of high excitation/inhibition balance in adult-born neurons. Science 335:1238–1242. CrossRef Medline

Mich JK, Signer RA, Nakada D, Pineda A, Burgess RJ, Vue TY, Johnson JE, Morrison SJ (2014) Prospective identification of functionally distinct stem cells and neurosphere-initiating cells in adult mouse forebrain. eLife 3:e02669. CrossRef Medline

Ming GL, Song H (2005) Adult neurogenesis in the mammalian central nervous system. Annu Rev Neurosci 28:223–250. CrossRef Medline

Mongiat LA, Espósito MS, Lombardi G, Schinder AF (2009) Reliable activation of immature neurons in the adult hippocampus. PLoS One 4:e5320. CrossRef Medline

Mori T, Tanaka K, Buffo A, Wurst W, Kühn R, Götz M (2006) Inducible gene deletion in astroglia and radial glia: a valuable tool for functional and lineage analysis. Glia 54:21–34. CrossRef Medline

Ninkovic J, Mori T, Götz M (2007) Distinct modes of neuron addition in adult mouse neurogenesis. J Neurosci 27:10906–10911. CrossRef Medline

Overstreet Wadiche L, Bromberg DA, Bensen AL, Westbrook GL (2005) GABAergic signaling to newborn neurons in dentate gyrus. J Neurophysiol 94:4528–4532. CrossRef Medline

Overstreet-Wadiche LS, Bensen AL, Westbrook GL (2006) Delayed development of adult-generated granule cells in dentate gyrus. J Neurosci 26:2326–2334. CrossRef Medline

Owens DF, Boyce LH, Davis MB, Kriegstein AR (1996) Excitatory GABA responses in embryonic and neonatal cortical slices demonstrated by gramicidin perforated-patch recordings and calcium imaging. J Neurosci 16:6414–6423. Medline

Paxinos G, Franklin KB (2004) The mouse brain in stereotaxic coordinates. San Diego: Academic.

Piatti VC, Espósito MS, Schinder AF (2006) The timing of neuronal development in adult hippocampal neurogenesis. Neuroscientist 12:463–468. CrossRef Medline

Piatti VC, Davies-Sala MG, Espósito MS, Mongiat LA, Trinchero MF, Schinder AF (2011) The timing for neuronal maturation in the adult hippocampus is modulated by local network activity. J Neurosci 31:7715–7728. CrossRef Medline

Piatti VC, Ewell LA, Leutgeb JK (2013) Neurogenesis in the dentate gyrus: carrying the message or dictating the tone. Front Neurosci 7:50. CrossRef Medline

Taupin P (2007) BrdU immunohistochemistry for studying adult neurogenesis: paradigms, pitfalls, limitations, and validation. Brain Res Rev 53:198–214. CrossRef Medline

Temprana SG, Mongiat LA, Yang SM, Trinchero MF, Alvarez DD, Kropff E, Giacomini D, Beltramone N, Lanuza GM, Schinder AF (2015) Delayed coupling to feedback inhibition during a critical period for the integration of adult-born granule cells. Neuron 85:116–130. CrossRef Medline

Toni N, Laplagne DA, Zhao C, Lombardi G, Ribak CE, Gage FH, Schinder AF (2008) Neurons born in the adult dentate gyrus form functional synapses with target cells. Nat Neurosci 11:901–907. CrossRef Medline

Ye GL, Yi S, Gamkrelidze G, Pasternak JF, Trommer BL (2005) AMPA and NMDA receptor-mediated currents in developing dentate gyrus granule cells. Brain Res Dev Brain Res 155:26–32. CrossRef Medline

Zhao C, Teng EM, Summers RG Jr, Ming GL, Gage FH (2006) Distinct morphological stages of dentate granule neuron maturation in the adult mouse hippocampus. J Neurosci 26:3–11. CrossRef Medline

Zhao C, Deng W, Gage FH (2008) Mechanisms and functional implications of adult neurogenesis. Cell 132:645–660. CrossRef Medline